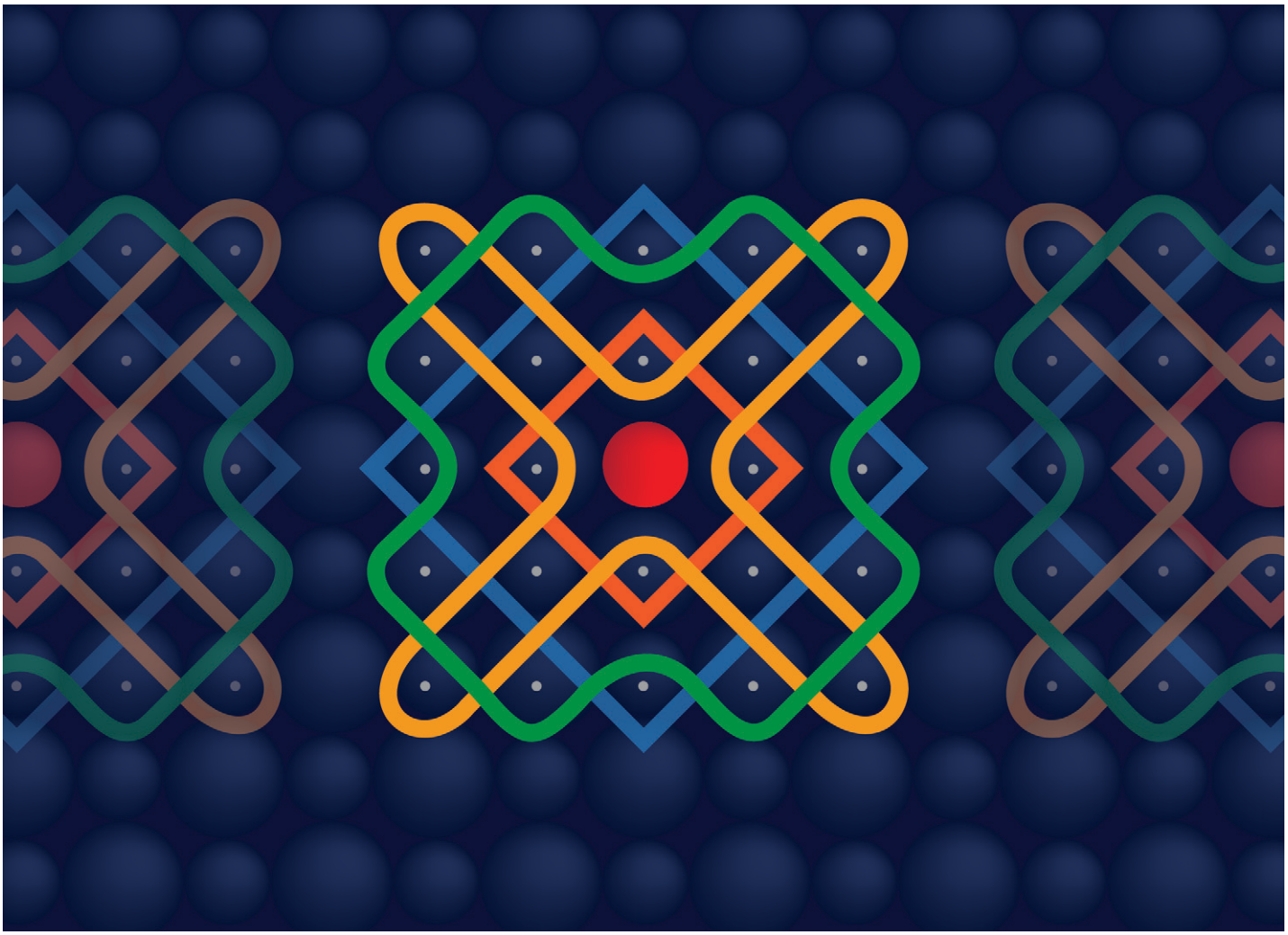

Highlighting the experiments from the Cat-Sense group, Department of Chemistry, Indian Institute of Technology Palakkad, Kerala and National Chemical Laboratory, Pune in India.

Oxidation of ethylene by Cu/TiO_2: reducibility of Cu^{2+} in TiO_2 as a possible descriptor of catalytic efficiency

The background of the image shows the crystal face of TiO_2. The red spheres that stand out represent Cu^{2+} dopant. The colourful geometrical pattern is inspired from the traditional folk-art form in south India called Kolam. It involves dots arranged in a specific manner like a grid around which free flowing strokes are drawn in a calculated manner to form an intricate pattern. The colourful pattern around the red sphere represents the multifunctional role of Cu^{2+} in the catalytic oxidation of ethylene.

Image credit: "Madhubaani Designs, Palakkad"

As featured in:

See Dinesh Jagadeesan *et al.*, *Catal. Sci. Technol.*, 2023, **13**, 2330.

ROYAL SOCIETY OF CHEMISTRY

rsc.li/catalysis

Registered charity number: 207890

Catalysis Science & Technology

ROYAL SOCIETY OF CHEMISTRY

PAPER

View Article Online
View Journal | View Issue

Cite this: *Catal. Sci. Technol.*, 2023, **13**, 2330

Oxidation of ethylene by Cu/TiO_2: reducibility of Cu^{2+} in TiO_2 as a possible descriptor of catalytic efficiency†

K. Rajendran, [a] Mandeep Sharma, [a] Augustine Jaison,[a] Menon Ankitha, [a] Ankit D. Tiwari,[a] C. P. Vinod [c] and Dinesh Jagadeesan *[ab]

Catalytic oxidation using non-noble metal-based catalysts is a promising approach to mitigate pollution due to VOCs in the air. In this work, mesoporous Cu/TiO_2 catalysts containing different concentrations of Cu^{2+} (0.2, 1, 3, and 4 wt% Cu w.r.t. Ti) were synthesized using the sol–gel technique. The catalysts were characterized using inductively coupled plasma-optical emission spectrometry, XRD, Raman spectroscopy, N_2 physisorption, cyclic voltammetry, H_2-TPR and electron microscopy to understand the structure and composition. The thermal catalytic gas phase oxidation of ethylene was studied by heating a mixture of ethylene (1.5 vol%) and air (5.9 vol%) in the presence of the Cu/TiO_2 samples in the temperature range of 298 to 773 K. Cu/TiO_2 showed a higher catalytic activity compared to TiO_2 for the thermal oxidation of ethylene, indicating a strong promotion by doped copper ions. A volcanic behaviour in the catalytic activity was observed with different concentrations of Cu doping, with 1% Cu/TiO_2 showing a 99.5% ethylene conversion at 673 K and 100% selectivity to CO_2. The activity of 1% Cu/TiO_2 remained consistent without deactivation for 24 h. At low dopant concentrations of Cu (0.2 and 1% Cu/TiO_2), the reduction of Cu^{2+} to Cu^{+} was observed. An interplay of oxygen vacancies (O_V), Cu^{+}, Cu^{2+} and Ti^{4+} may be involved in controlling the activity. DRIFT studies indicated the formation of surface bidendate carbonate as a possible intermediate.

Received 27th December 2022,
Accepted 9th March 2023

DOI: 10.1039/d2cy02170f

rsc.li/catalysis

1. Introduction

In 2022, the *Global Burden of Diseases* reported air pollution as the single highest risk factor for tracheal, bronchial, and lung cancer among vulnerable populations.[1] In recent years, various anthropogenic activities have led to a substantial increase in the concentration of atmospheric volatile organic compounds (VOCs).[2–4] Particularly, the presence of ethylene in air is closely linked to the high likelihood for the formation of photochemical smog. Besides, ethylene in air is also responsible for the large-scale spoilage of fruits and vegetables during storage in warehouses. Mitigation of VOCs such as ethylene is therefore a problem with a wider social and economic impact.[5] Complete mitigation of ethylene by chemical oxidation to CO_2 (and not to CO or ethylene oxide) by catalytic technology is a promising approach.[6–8] Catalysts based on noble metals such as Ru, Pd, Pt and Au have been reported to have the best rates of ethylene oxidation in the temperature range of 323–493 K.[9–12] However, the high costs and vulnerability to poisoning of noble metals remain as bottlenecks to their scalability. As a result, catalysts based on transition metals and their oxides have been actively considered as viable alternatives.[6,8,13,14] In this work, we have explored the catalytic activity of Cu doped TiO_2 for ethylene oxidation.

Catalytic oxidation of a VOC by a metal oxide operates *via* the Mars–van Krevelen mechanism, which necessitates the involvement of oxygen vacancies (O_V).[15] In addition to O_V, the Lewis acidity of cations may also be helpful to anchor the incoming unsaturated hydrocarbon.[16] TiO_2 is a thermally stable material that is commonly used as a support for active metal catalysts in reactions.[17–20] With motivation to develop new transition metal oxide-based catalysts, we suspected that doping a low valent transition metal ion such as Cu^{2+} into the matrix of a reducible oxide such as TiO_2 could lead to an interesting catalytic system. The imbalance in charge and size between Cu^{2+} and Ti^{4+} ions can create labile O atoms in the vicinity of the dopant, thereby decreasing the energy of formation of O_V.[21] Besides, the Lewis acidity of the cations (Cu^{2+} and Ti^{4+}) could increase the adsorption of ethylene.

[a] *Department of Chemistry, Indian Institute of Technology Palakkad, Kerala, 678557, India. E-mail: d.jagadeesan@iitpkd.ac.in*
[b] *Environmental Sciences and Sustainable Engineering Centre (ESSENCE), Indian Institute of Technology Palakkad, Kerala, 678557, India*
[c] *Inorganic Chemistry and Catalysis Division, CSIR – National Chemical Laboratory, Pashan, Pune – 411 008, Maharashtra, India*
† Electronic supplementary information (ESI) available. See DOI: https://doi.org/10.1039/d2cy02170f

Cu^{2+} was chosen as a dopant due to Cu–O bonds on the catalyst surface being able to activate C–H bonds.[22,23] Although many Cu based catalysts have been used in the past for ethylene oxidation, a majority of them were used in combination with highly redox active metals such as Ce and Mn.[8,13,14] In this work, we have synthesized Cu/TiO_2 with various concentrations of Cu^{2+} ions (0.2, 1, 3, 4 wt% Cu w.r.t. Ti) and systematically studied the role of Cu in creating active sites for ethylene oxidation. It is demonstrated that Cu^{2+} can promote TiO_2 resulting in an enhancement in the oxidation of ethylene to CO_2 in the range of 500–600 K. To the best of our knowledge, there has not been any report on the catalytic thermal oxidation of ethylene using Cu doped TiO_2 (Cu/TiO_2).

2. Experimental section

2.1 Materials

Titanium butoxide $Ti(OC_4H_9)_4$ 97%, glacial acetic acid CH_3-COOH 99%, ethanol C_2H_5OH 99.5%, hydrochloric acid HCl 37%, Pluronic F127, and copper sulphate pentahydrate $CuSO_4{\cdot}5H_2O$ 99.995%. The above chemicals were obtained from Sigma-Aldrich and NICE.

2.2 Synthesis of materials

The sol–gel method was used for the synthesis of Cu/TiO_2. In 30 mL ethanol, 1.6 g of Pluronic F127 was added along with 2.3 mL acetic acid and 0.74 mL HCl. Following this, 3.5 mL titanium butoxide and $CuSO_4{\cdot}5H_2O$ (Table S1†) were mixed. The mixture was stirred vigorously for 1 h and then transferred to a Petri dish, which was later kept in an oven for 12 h at 313 K and at 338 K for 24 h for aging. The sample was pulverized and calcined at 773 K for 4 h at a ramp rate of 1 °C min^{-1} to remove the surfactants to get mesoporous Cu/TiO_2.

2.3 Ethylene oxidation activity measurement

Ethylene oxidation was carried out using 0.08 g (0.2, 1, 3, 4 wt%) Cu/TiO_2 loaded in a 1/4″ stainless steel tube in a vertical furnace. A total flow rate of 10 mL min^{-1} with 7.15 mL min^{-1} for ethylene (1.5 vol%) and 2 mL min^{-1} for air (5.9 vol%) was maintained using digital mass flow controllers. A hourly space velocity of 3157.9 h^{-1} was maintained throughout the experiment. The unreacted ethylene and products were analysed using an Agilent 7890B gas chromatograph (GC) equipped with a thermal conductivity detector (TCD) and a flame ionization detector (FID). The ethylene conversion, selectivity to CO_2 and turnover number were calculated using eqn (1), (2) and (3), respectively.

$$\text{Ethylene conversion} = \frac{([C_2H_4]\text{Initial} - [C_2H_4]\text{Final})}{[C_2H_4]\text{Initial}} \times 100 \quad (1)$$

$$\text{Selectivity to } CO_2 = \frac{\text{Moles of } CO_2 \text{ produced}}{\text{Moles of ethylene converted}} \times 100 \quad (2)$$

$$\text{Turnover number} = \frac{\text{Moles of ethylene converted}}{\text{Moles of Copper}} \quad (3)$$

2.4 Characterization of materials

A Rigaku Smart Lab X-ray diffractometer was used for the analysis of the crystalline phase of the catalysts with Cu Kα radiation (λ = 0.154 nm) in the range of 2θ = 20–80 degrees, operated at a current of 200 mA and a voltage of 45 kV. Raman spectra of the catalysts were examined using a Horiba Labram spectrometer with a 532 nm ultra-low frequency laser source. A Quantachrome Chemstar TPX chemisorption instrument was used to check the reducibility of the catalysts. Temperature programmed reduction (H_2-TPR) of samples was carried out in a 10% H_2/Ar flow (used as the reducing atmosphere) and heated from room temperature to 1073 K at 10 K min^{-1}. The H_2 consumption of 0.6 mg of catalyst for the reduction process was monitored using a TCD at different temperature intervals. The surface elemental composition of the catalyst was analysed by X-ray photoelectron spectroscopy (XPS) using a K ALPHA+ (Thermo Fisher Scientific Instruments, UK). Monochromatic Al Kα was used as the X-ray source at a 6 mA beam current and 12 kV. Inductively coupled plasma-optical emission spectrometry (ICP-OES) was used to calculate the wt% of Cu in TiO_2. N_2 physisorption was performed at liquid N_2 temperature using a Quantachrome Autosorp IQ-MP and Brunauer–Emmett–Teller (BET) analysis was carried out to determine the surface area, average pore size and total pore volume. Transmission electron microscopy (TEM) was used for the analysis of the microstructure of the material. The Cu/TiO_2 samples were electrochemically investigated by performing cycling voltammetry studies on a CHI60038 electrochemical workstation. The setup has a 3-electrode system in which a Cu/TiO_2 coated glassy carbon electrode (GCE) (diameter 3 mm, area 0.07 cm^2) was used as the working electrode, a Pt wire as the counter electrode, and a saturated calomel electrode (SCE) as the reference electrode. A catalyst ink for the electrochemical studies was prepared by sonicating 10 mg of the Cu/TiO_2 catalyst in a water–ethanol (1 : 1) mixture containing 100 μL of Nafion (0.5 wt% in a solution of 1 : 1 water–ethanol) to a final concentration of 10 mg mL^{-1} of the catalyst. Thereafter, 6 μL of the catalyst ink (0.06 mg) was drop cast onto a GCE and allowed to dry under ambient conditions. Cyclic voltammetry studies were carried out at a scan rate of 50 mV s^{-1} with 0.50 M Na_2SO_4 as the electrolyte at room temperature. *In situ* diffuse reflectance infrared Fourier transform spectroscopy (DRIFTS) was performed on a FT-IR spectrometer (Shimadzu IR Tracer 100), equipped with a diffuse reflectance accessory and a DLATGS (deuterated L-alanine doped triglycine sulphate) detector. The DRIFTS reaction chamber is made of stainless steel with a ZnSe window.

3. Results and discussion

3.1 Characterization of Cu doped TiO_2 (Cu/TiO_2)

Cu/TiO_2 catalysts containing different concentrations of the Cu dopant were prepared using the sol–gel method. In Fig. 1a trace (i), the powder XRD peaks revealed the anatase phase of TiO_2 (ICSD code: 98-000-5224) with the (011), (004), (020), (015), (121), (024), (116), (220) and (125) planes. Interestingly, none of the peaks in the XRD patterns of Cu/TiO_2 samples (traces ii to v) could be indexed to any of the bulk CuO phases. This observation has been reported by earlier researchers too.[24] This indicated that either the CuO phase was too small to be detected by XRD or Cu existed in the form of highly dispersed ions in the TiO_2 matrix. The suspicion behind the high dispersion of Cu in the TiO_2 matrix is justified due to the excellent stabilization of Cu^{2+} during the condensation of the precursors in sol–gel synthesis.[25,26] An interesting observation was the broadening of the (011) peak of the Cu/TiO_2 samples. From the width of the XRD peak, it was estimated that the average crystallite size decreased from 10.3 nm for pure TiO_2 to 7.4 nm for 4% Cu/TiO_2 as shown in Table S2.† A slight shift of 0.2 degrees in two theta of the (011) plane was observed in 1% Cu/TiO_2. Generally, a shift in the peak position may be attributed to a change in lattice parameters of the unit cell which could arise due to the doping of an ion, whose radius may vary by more than 10–15% of the radii of the native ions of the lattice, $r_{Ti^{4+}}$ (0.68 Å) < $r_{Cu^{2+}}$ (0.72 Å).[27] Fig. 1b elucidates the Raman spectra of undoped TiO_2 and Cu/TiO_2 samples. Trace i) corresponding to pure TiO_2 displayed bands at 144.9, 197.4, 399.2, 516.6 and 639.2 cm^{-1}, which are indexed to the anatase structure of titania.[28] The Cu/TiO_2 samples with different concentrations of Cu gave identical bands in the Raman spectra, indicating that the anatase phase of TiO_2 was retained in all cases. Interestingly, the E_g mode at 144.9 cm^{-1}, which is assigned to the symmetric stretching of Ti–O bonds, showed a redshift with increasing concentration of Cu in TiO_2 (see Fig. S1†). The reduction in the particle size probably created more under-coordinated surface sites.[24] This shrinkage of crystallite size with increasing concentration of Cu corroborated well with the XRD results. The effect of Cu doping resulted in the formation of new bonds such as Cu–O–Ti or Cu–O–Cu. An imbalance of charges across the new bonds can create oxygen vacancies.[21] As a result, the Raman spectra clearly indicated the softening of the vibrational modes in the form of a red shift of the E_g mode. Similar results were observed earlier too.[24]

Having confirmed that doping of Cu neither affected the phase purity in TiO_2 nor caused any phase separation, the temperature programmed chemisorption technique was employed to probe the nature of Cu and its interaction with the TiO_2 matrix. H_2-TPR was carried out to understand the ease of reduction of Cu^{2+} ions in the TiO_2 matrix. H_2-TPR profiles of bare TiO_2 and Cu doped TiO_2 samples are shown in Fig. 2a. Three thermally induced reduction events occur in the temperature range of 400 to 1000 K. The reduction of Cu^{2+} to Cu^{+} occurs in the temperature range of 400–550 K (pink region), while that of Cu^{+} to Cu^{0} occurs in the range of 550–650 K (green region) and Ti^{4+} to Ti^{3+} above 700 K (as a doublet, purple region).[26,29] The curve corresponding to 0.2% Cu/TiO_2 (trace ii) did not show significant difference in features compared to that of pure TiO_2 (trace i). Although the concentration of Cu^{2+} may not be high enough to cause a noticeable reduction peak, the presence of traces of Cu^{0} after H_2 reduction (during the H_2-TPR experiment) may accelerate the reduction of Ti^{4+} to Ti^{3+}.[30] As a result, one can note that the positions of doublet peaks (Ti^{4+} to Ti^{3+}) migrate to a lower temperature with increasing concentration of Cu. The narrower peak in the 550–650 K region in 1% Cu/TiO_2 (trace iii) is indicative of the reduction of Cu^{+} to Cu^{0}. Although not very distinct, there could also be the reduction of Cu^{2+} to Cu^{+} happening, as seen by the asymmetry of the peak.[31]

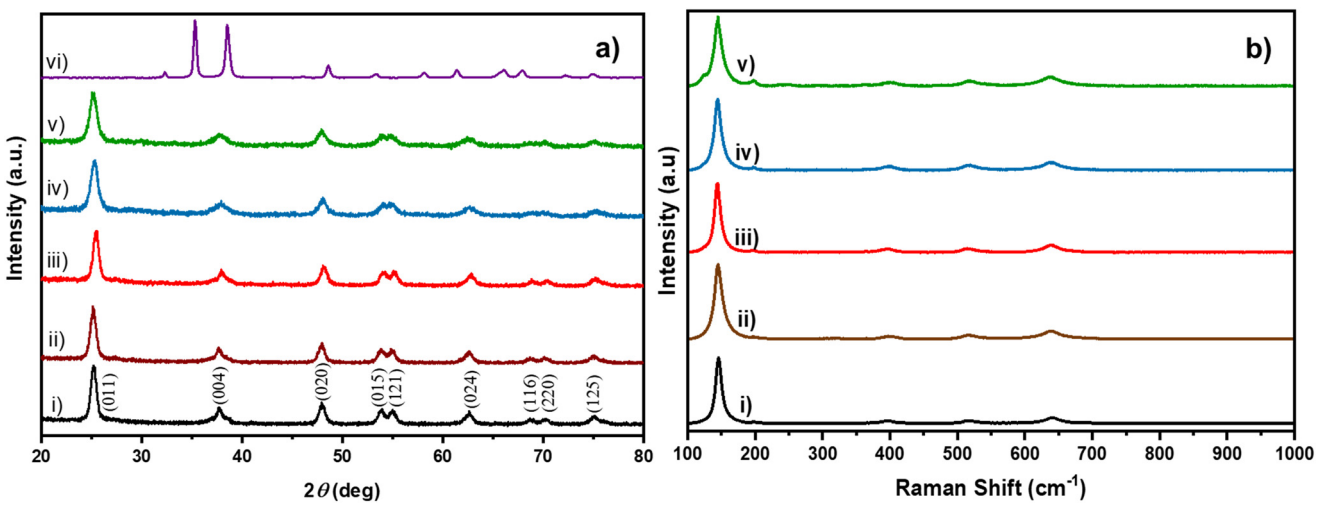

Fig. 1 a) XRD patterns of i) TiO_2 (black), ii) 0.2% Cu/TiO_2 (brown), iii) 1% Cu/TiO_2 (red), iv) 3% Cu/TiO_2 (blue), v) 4% Cu/TiO_2 (green) and vi) bulk CuO (violet). b) Raman spectra of i) TiO_2 (black), ii) 0.2% Cu/TiO_2 (brown), iii) 1% Cu/TiO_2 (red), iv) 3% Cu/TiO_2 (blue) and v) 4% Cu/TiO_2 (green).

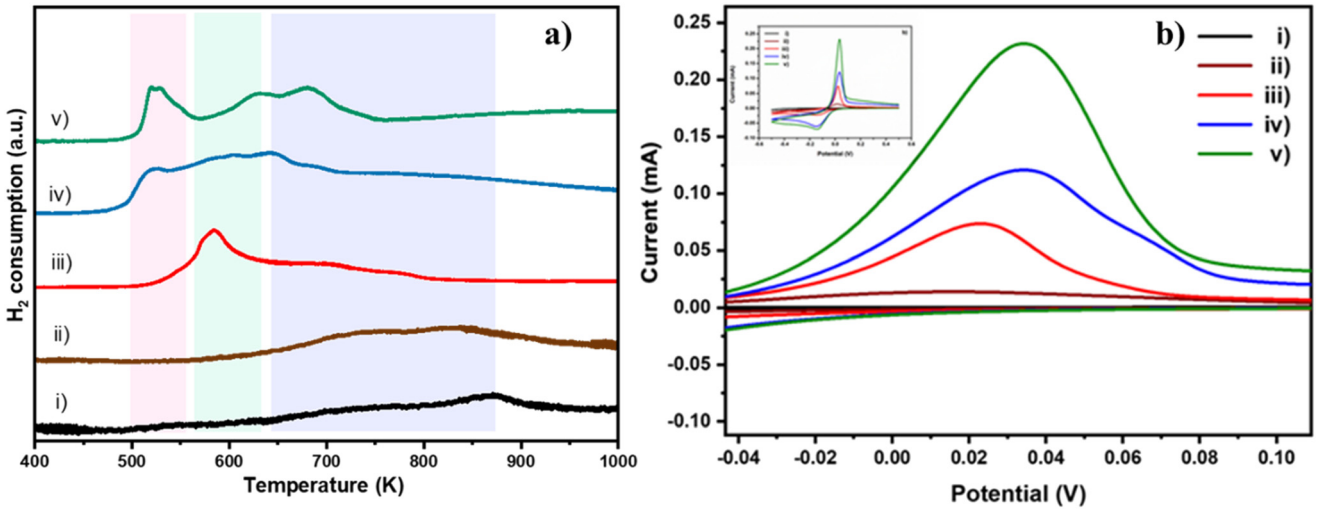

Fig. 2 a) H_2-TPR curves of i) TiO_2, ii) 0.2% Cu/TiO_2, iii) 1% Cu/TiO_2, iv) 3% Cu/TiO_2 and v) 4% Cu/TiO_2. Colour bands represent the following reduction events: pink band on the left side (Cu^{2+} to Cu^{+}), green band in the middle (Cu^{+} to Cu^{0}) and purple band on the right (Ti^{4+} to Ti^{3+}). b) CV profiles at a scan rate of 50 mV s^{-1} for the different samples: i) TiO_2 (black); ii) 0.2% Cu/TiO_2 (brown); iii) 1% Cu/TiO_2 (red); iv) 3% Cu/TiO_2 (blue); v) 4% Cu/TiO_2 (green). Inset shows the CV profiles of oxidation and reduction potential of the samples recorded at 50 mV s^{-1} over the potential range −0.5 to +0.5 V.

Importantly, as shown in Table S3 in the ESI,† the low temperature peak due to the reduction of copper ions is shifted to further lower temperatures as the concentration of Cu increased, suggesting that the reduction of Cu^{2+} is a more favourable process at higher concentrations. A concomitant shift in the position of the doublet also supports our observation that the availability of Cu^0 becomes higher as the concentration of Cu is increased.[30] Analysis of the ratio of Cu^{2+}/Cu^{+} based on the volume of H_2 consumed (Table S4 in the ESI†) revealed that at low dopant concentration, Cu^{2+} is reduced to Cu^{+} due to strong metal–support interaction. However, as the concentration increases, in addition to the existence of Cu^{+}, the stabilization of Cu^{2+} is gradually improved leading to the co-existence of Cu^{+} and Cu^{2+}. A slight shift in the position of reduction peaks of both Cu^{2+} and Ti^{4+} to higher temperature (for 4% Cu/TiO_2) indicated that Cu^{2+} was probably stabilized making its reduction difficult.

This concentration dependent redox behaviour of Cu in TiO_2 was also followed using cyclic voltammogram (CV) studies (Fig. 2b). CVs were obtained in a cathodic sweep at a scan rate of 50 mV s^{-1}, followed by an anodic sweep at the same scan rate. The anodic and cathodic peaks are attributed to the oxidation of Cu^{+} to Cu^{2+} and reduction of Cu^{2+} to Cu^{+} respectively.[32] As expected, pure TiO_2 did not exhibit any distinct redox peaks in the scanning range of −0.5 V to 0.5 V. The oxidation peak occurred at 0.016 V in the 0.2% Cu/TiO_2 curve (ii). In the 1% Cu/TiO_2 curve (iii), the oxidation peak shifted by 5 mV to 0.021 V. In the 3% Cu/TiO_2 curve (iv), it increased further to 0.034 V. A very slight shift to a lower potential was observed for 4% Cu/TiO_2, which was consistent with the H_2-TPR data curve (v). The data suggested that the ease of oxidation of Cu^{+} to higher oxidation states increased with decreasing concentration of the dopant from 3 to 0.2% Cu/TiO_2. Both H_2-TPR and CV studies suggested the better redox characteristics of Cu/TiO_2 compared to those of pure TiO_2. The ease of reducibility of Cu^{2+} increased with the increase in the concentration of the dopant. The redox behaviour of Cu/TiO_2 is a promising feature of the oxidation ability of the catalysts.

3.2 Catalytic activity of Cu/TiO_2

Fig. 3a shows the catalytic performance of Cu/TiO_2 for the oxidation of ethylene at various temperatures. The oxidation of ethylene over undoped TiO_2 began at 573 K but did not reach 100% conversion even after reaching 750 K. In contrast, the ethylene conversion by Cu/TiO_2 typically started at 423 K and improved to 70% conversion at 550 K. At 623 K, 3% Cu/TiO_2 showed a 99% ethylene conversion, while 1% and 4% Cu/TiO_2 gave a 90% and 99% conversion, respectively. Most importantly, in all the samples, CO_2 was formed with 100% selectivity. Although the temperature dependent activity was more or less similar for the various Cu/TiO_2 samples, the 3% and 4% samples achieved complete conversion at a slightly lower temperature. 3% Cu/TiO_2 is the most active catalyst in all the temperature ranges. The oxidation ability of the Cu/TiO_2 catalyst corroborated well with the H_2-TPR and CV studies. Interestingly, even the subtle change in the trend of the reducibility of Cu^{2+} in the 3% and 4% samples could be correlated with an observable outcome in terms of catalytic activity. The efficiency of the catalyst was further understood by plotting the turnover number (TON) which represents the number of moles of ethylene converted by a mole of copper at a given temperature (Fig. 3b). At 573 K, where the activity began, 1% Cu/TiO_2 showed a high TON of 6.9×10^{-3} compared to that of 0.2% (1.6×10^{-3}), 3% (2.9×10^{-3}) and 4% (2.1×10^{-3}).

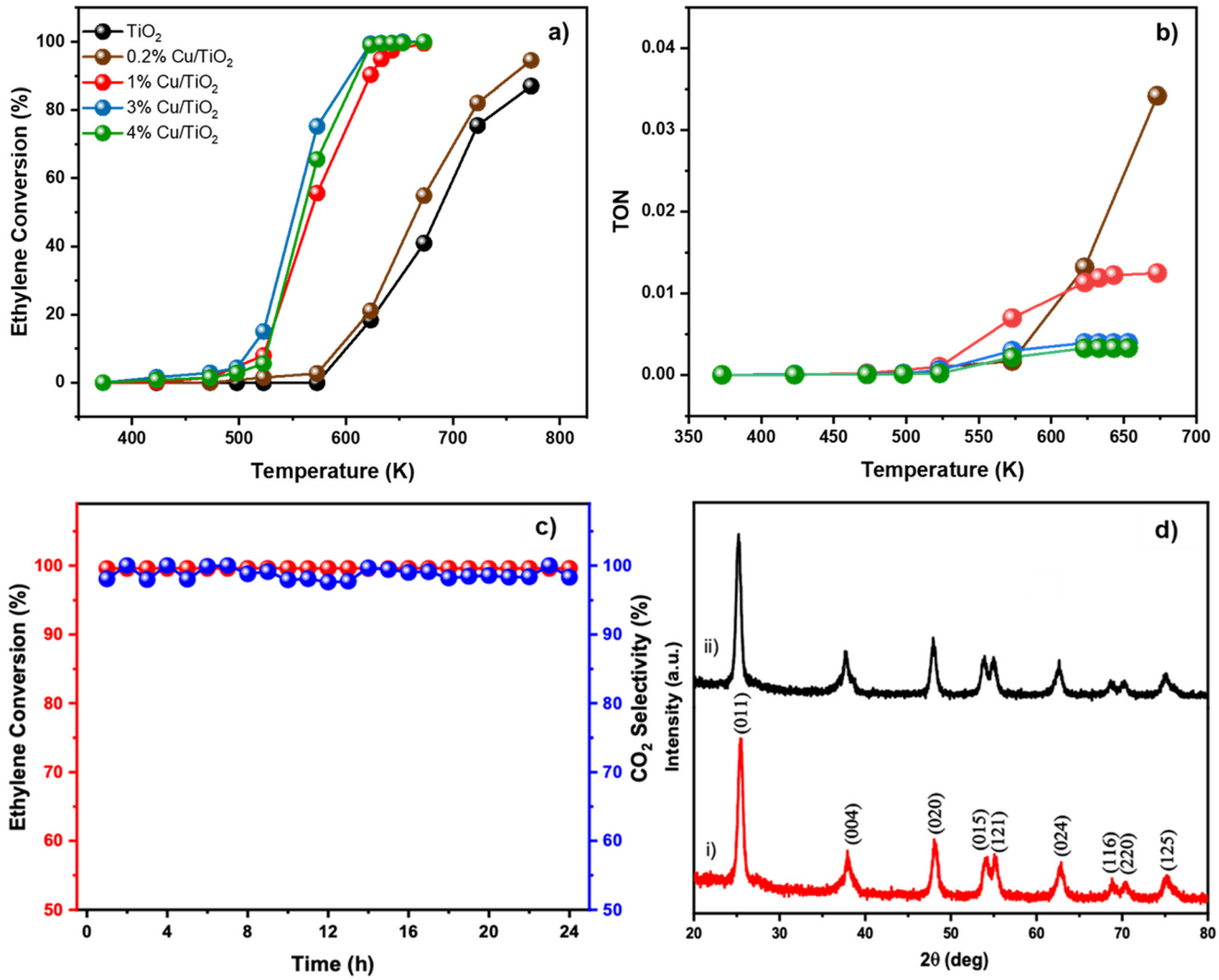

Fig. 3 a) Plots of ethylene conversion (%) against temperature (K) for TiO_2 and Cu doped TiO_2 samples (0.2%, 1%, 3% and 4%). Inset shows the colour coding for the various samples TiO_2 (black), 0.2% Cu/TiO_2 (brown), 1% Cu/TiO_2 (red), 3% Cu/TiO_2 (blue) and 4% Cu/TiO_2 (green). b) Plots of turnover number (TON) of Cu doped TiO_2 samples against temperature (K). The colour legend is same as that in a). c) Thermal stability of 1% Cu/TiO_2 demonstrated by monitoring the conversion of ethylene at 673 K for 24 h. d) XRD patterns of 1% Cu/TiO_2 i) before reaction and ii) after reaction for 24 h.

Expectedly, as the temperature increased, the TON increased too and reached a saturation value at around 623 K. The TON value for 1%, 3% and 4% Cu/TiO_2 was 1.13×10^{-2}, 3.91×10^{-3} and 3.26×10^{-3} respectively. This temperature also correlated with a 100% conversion of ethylene. Interestingly, the activity of 0.2% Cu/TiO_2 started at around 573 K but it reached a high TON of 1.3×10^{-2} at 623 K. At 673 K, when most of the other compositions had reached a saturation in conversion, the TON of 0.2% Cu/TiO_2 reached 3.4×10^{-2}, which was three times higher than that of 1% Cu/TiO_2. Intriguingly, the TON value for 0.2% did not reach saturation even beyond 673 K. Although the temperature of conversion of 0.2% Cu/TiO_2 was higher compared to those of other Cu/TiO_2 compositions, the interesting observation presents scope for more in-depth structural correlation studies. Convincingly, the results indicated that the activity of Cu/TiO_2 was significantly higher than that of pure TiO_2 for the oxidation of ethylene suggesting the promotional effect of Cu on TiO_2.

The thermal stability of 1% Cu/TiO_2 was studied by carrying out the ethylene conversion at 673 K over 24 h continuously. In Fig. 3c, the conversion of ethylene and selectivity to CO_2 remained at 100% throughout the time on stream. This indicated that no deactivation happened during the continuous operation at elevated temperatures. In Fig. 3d, the XRD pattern of 1% Cu/TiO_2 after reaction for 24 h was compared with the XRD pattern before the reaction. There was no sign of phase separation indicating the excellent thermal stability of the catalyst. Considering the practicality of the process, 1% Cu/TiO_2 displayed the best TON at a reasonable temperature. The structure of 1% Cu/TiO_2 was examined using TEM. Spherical nanoparticles (Fig.

S3†) were observed in the TEM micrographs. The average particle size of 1% Cu/TiO_2 varied from 8–12 nm, which is close to the 9.76 nm crystallite size of 1% Cu/TiO_2 as calculated from XRD using the Debye–Scherrer equation (Table S2†). The *d*-spacing was calculated as 0.35 nm from the lattice fringes, corresponding to the (011) plane of the anatase TiO_2 phase in XRD.

3.3 Probing the active sites

One of the important impacts of doping Cu^{2+} in TiO_2 is the creation of O_V. Substitution of a larger Cu^{2+} ion (72 pm) for Ti^{4+} (65 pm) in TiO_2 is likely to introduce strain as well as charge imbalance in the lattice, which may be alleviated by forming an O_V.[24,33,34] To confirm the presence of O_V, XPS spectra were obtained for all the Cu/TiO_2 compositions. Two peaks were observed in the Ti spectra (Fig. S4†) at 458.4 eV and 464.08 eV, corresponding to $2p_{3/2}$ and $2p_{1/2}$, respectively. This confirms the presence of Ti^{4+} in all the samples of Cu/TiO_2.[35]

The Cu 2p XPS spectra of the different Cu/TiO_2 samples are shown in Fig. 4a. In the literature, peaks at 932.5 eV for Cu $2p_{3/2}$ and 952.0 eV for Cu $2p_{1/2}$ are taken as confirmation of the presence of Cu^+ species.[35] Similarly, peaks at 935.0 eV (Cu $2p_{3/2}$) with satellite peaks at 940.7 and 944.0 eV are a confirmation of the presence of Cu^{2+}. In the 0.2% Cu/TiO_2 sample trace (i), the Cu species are clearly in +1 state as the satellite peaks which are characteristic of Cu^{2+} are absent. In the 1% Cu/TiO_2 sample, Cu^+ could be the dominant species. A hump of very low intensity in the satellite peak region (Cu^{2+}) and a small tail peak at 935 eV (as shown in Fig. 4b) in 1% Cu/TiO_2 raise suspicion about the presence of Cu^{2+} as well. With further increasing Cu concentration, the presence of Cu^{2+} is established beyond doubt in TiO_2 along with Cu^+. The valence ratio (Cu^{2+}/Cu^+) of 1%, 3%, and 4% Cu/TiO_2 as calculated using XPS was 0.2, 0.5, and 0.9, respectively (Table S6†). An increase in the valence ratio (Cu^{2+}/Cu^+) was observed with the increase of Cu doping into TiO_2. The data suggest a strong metal–support interaction between Cu^{2+} and the TiO_2 matrix resulting in the reduction of Cu^{2+} to Cu^+ at low concentrations, which is firmly in agreement with the H_2-TPR and CV data. However, as the concentration increases, the interaction with the support is probably weakened leading to a higher presence of Cu^{2+} as well. The O 1s XPS spectra of the pure TiO_2 and Cu/TiO_2 samples are shown in Fig. 5a–e. The peak observed at 529.7 eV corresponds to the lattice oxygen (O_L) in the TiO_2 matrix. The second peak at 531.1 eV is due to the hydroxyl groups adsorbed on the surface (O_A).[24] The peak appearing at 532.1 eV is due to the chemisorbed oxygen created due to the presence of O_V.[24] Fig. 5a suggests that the undoped TiO_2 sample does not have O_V sites. On doping Cu into the TiO_2 lattice, the formation of O_V was observed. The percentage area due to O_V calculated with respect to the total area of the O 1s spectrum for the different samples (in brackets) suggested an increase in the surface O_V with the doping of Cu: 3 (0.2%), 10 (1%), 16 (3%) and 29 (4%). There is a direct correlation between the concentration of the surface O_V and the concentration of Cu in the TiO_2 matrix (Fig. 5f).

The acidity of the sample could also aid in a better adsorption of ethylene resulting in increased oxidation.[16] Pyridine DRIFTS was performed to probe the acidic sites on the most active 1% Cu/TiO_2 sample.[36–39] Initially, the sample was heated at 473 K in an inert atmosphere to remove the impurities on the surface followed by pyridine injection at 323 K. The spectrum is shown in Fig. 6a(i). The major peaks observed at 1445 cm^{-1}, 1574 cm^{-1}, and 1609 cm^{-1} correspond to Lewis acidic sites.[36,38] The peaks at 1540 and 1640 cm^{-1}

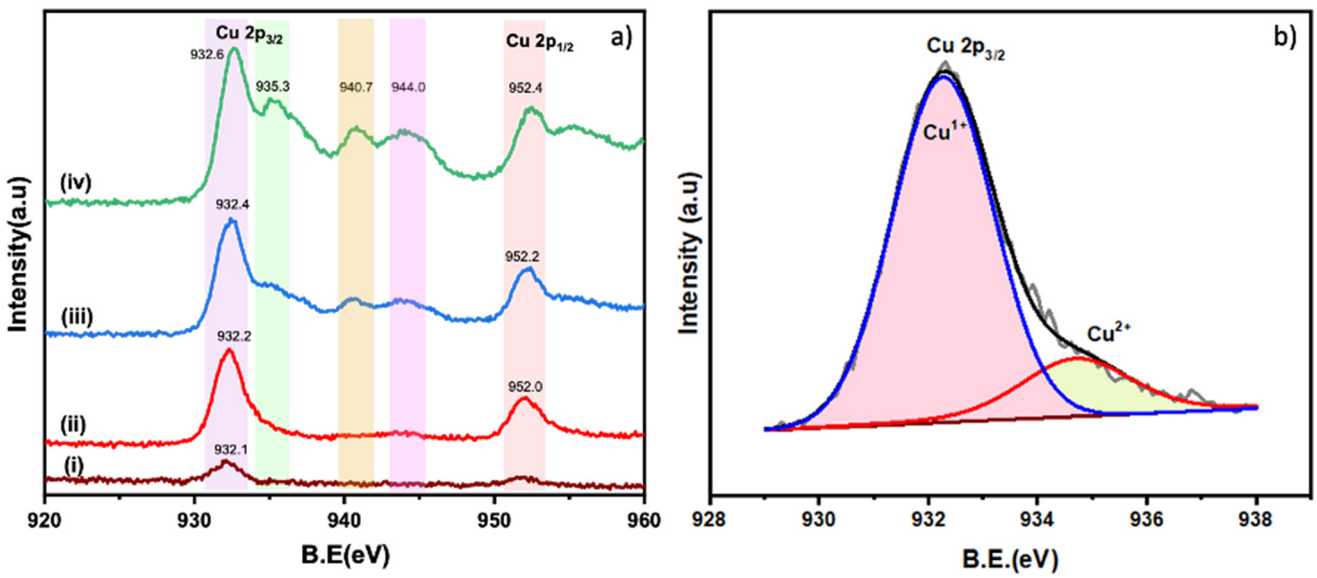

Fig. 4 a) XPS spectra of Cu 2p: i) 0.2% Cu/TiO_2, ii) 1% Cu/TiO_2, iii) 3% Cu/TiO_2 and iv) 4% Cu/TiO_2; b) deconvoluted spectrum of Cu $2p_{3/2}$ of 1% Cu/TiO_2.

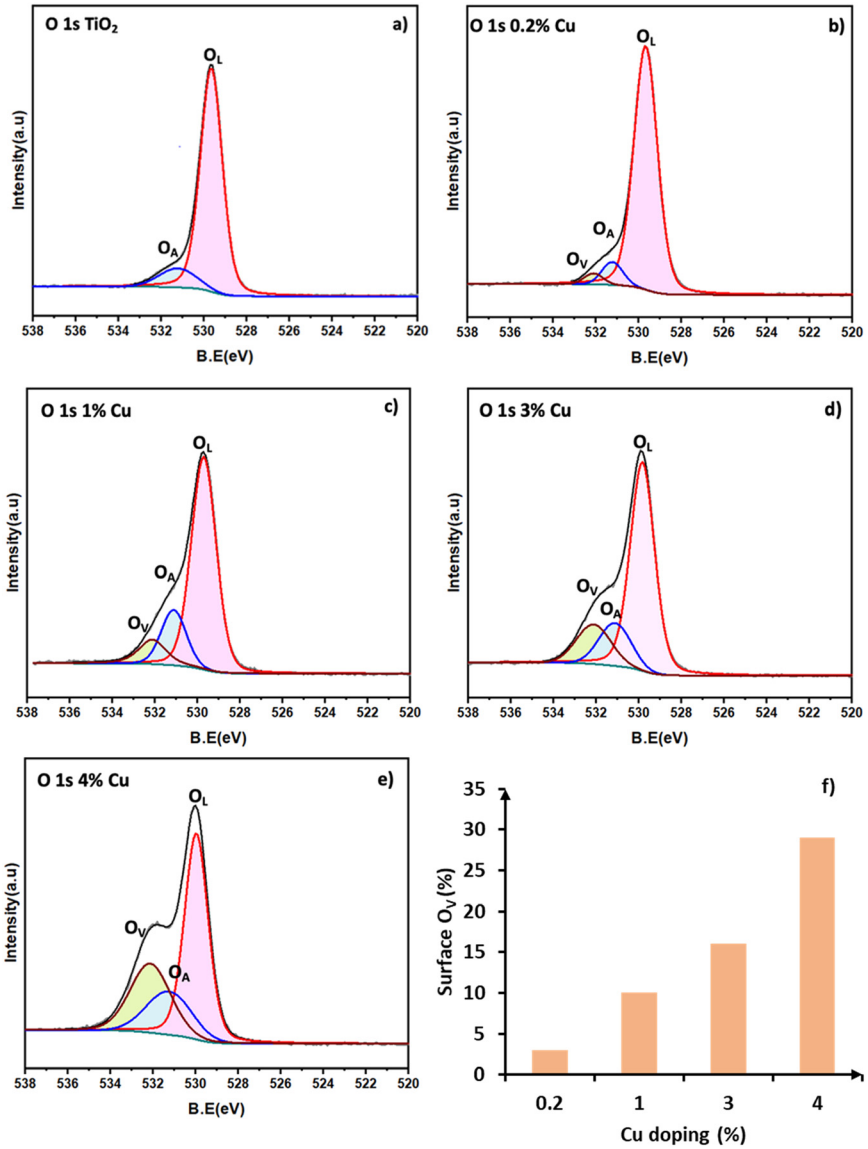

Fig. 5 X-ray photoelectron spectra of O 1s: a) TiO_2, b) 0.2% Cu/TiO_2, c) 1% Cu/TiO_2, d) 3% Cu/TiO_2 and e) 4% Cu/TiO_2. f) Correlation between surface O_V (normalized area in XPS) and doping concentration.

represent the presence of Brønsted acidic sites. The band at 1490 cm^{-1} indicates both Lewis and Brønsted acidic sites.[37] The bands were monitored by an increase in the temperature from 323 to 573 K under a N_2 atmosphere. The desorption of pyridine was not observed even at high temperatures (Fig. 6a(ii) to (iv)), suggesting the presence of strong acidic sites in 1% Cu/TiO_2.[37] Importantly, pyridine DRIFTS carried out on bare TiO_2 did not reveal the presence of strong acidic sites, clearly indicating the impact of doping of Cu into TiO_2 (Fig. S7†). In the next step, ethylene/air-DRIFTS was performed to probe the surface species that form on the Cu/TiO_2 during the reaction (Fig. 6b). Initially, the surface was purged with a N_2 atmosphere for an hour at 373 K to avoid signals due to impurities. A mixture of ethylene (1.5 vol%) and air (5.9 vol%) having an identical feed ratio to those in the reactions was used. The IR spectrum was recorded from 298 to 673 K in a continuous flow of feed gas. The band observed at around 1524 cm^{-1} corresponds to the scissoring mode δ(HCH) of the ethylene molecules at 298 K. Trace (ii) clearly showed the band corresponding to the adsorption of ethylene on the surface of the catalyst. The bands at 2330 and 2370 cm^{-1} indicate the stretching mode of gaseous CO_2. Moreover, the peak at 2350 cm^{-1} indicates the presence of adsorbed CO_2 on metal atoms.[40] As the temperature of the catalyst was increased, the band of δ(HCH) corresponding to the ethylene peaks disappeared and the band of ν(COC) and adsorbed CO_2 increased confirming the complete oxidation of ethylene to CO_2. The peak observed in the region of 1220 and 1350 cm^{-1} corresponds to the symmetric stretching of adsorbed bicarbonate and bidentate carbonate species on the metal oxide.[41] The same band started to disappear when the temperature was increased from 298 to 673 K. However, it

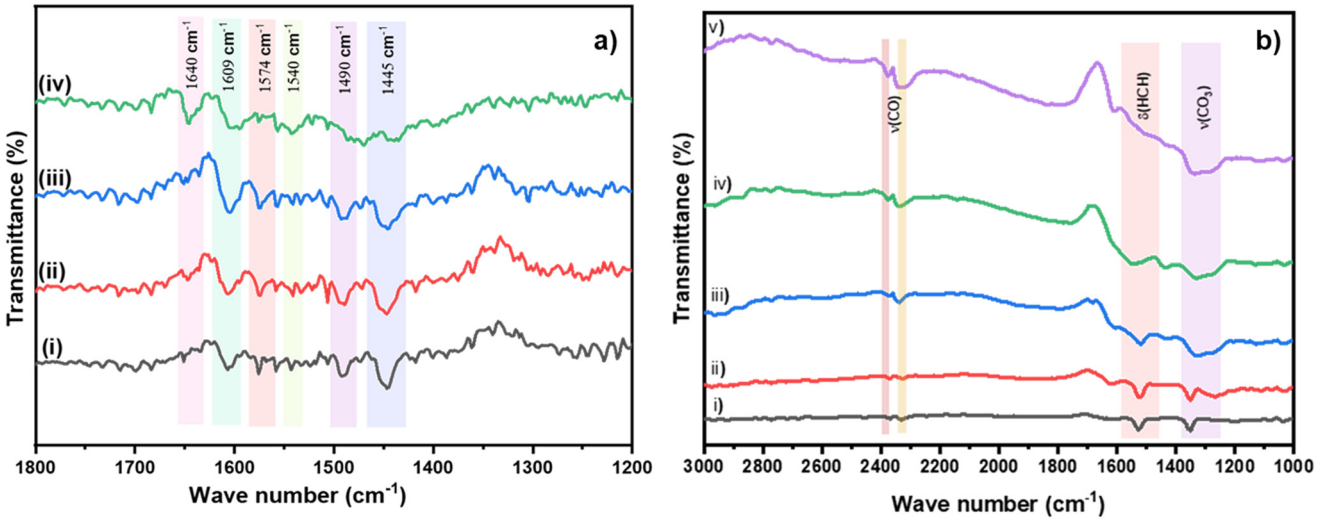

Fig. 6 a) Pyridine DRIFTS spectra of Cu/TiO_2 at (i) 323 K, (ii) 373 K, (iii) 473 K and (iv) 573 K. b) DRIFTS measurements during oxidation of ethylene using 1% Cu/TiO_2 with a mixture of ethylene (1.5 vol%) and oxygen (5.9 vol%) at (i) 298 K; (ii) 373 K; (iii) 473 K; (iv) 573 K; (v) 673 K.

was not clear whether carbonates were formed due to the re-adsorption of CO_2 or as an intermediate during the oxidation of ethylene. CO_2 gas was passed over the catalyst surface and spectra were recorded at different temperatures (Fig. S5†). No peaks corresponding to the formation of carbonates were observed from RT to 673 K in CO_2 DRIFTS.[42] The results indicate that carbonates were formed as an intermediate during the oxidation, not by the re-adsorption of CO_2. Moreover, the peak corresponding to –OH stretching in H_2O is shown in Fig. S6.† This could be due to the adsorption of water formed during the oxidation of ethylene. Despite this observation, the activity did not decrease up to 24 h. This indicates that despite the interaction of H_2O with the surface of the catalyst, the activity of the catalyst was unaffected. Although detailed surface studies are needed to understand the mechanism of ethylene oxidation, the DRIFT studies strongly indicate the oxidation occurring *via* the carbonate pathway.

The role of O_V in an oxidation reaction as explained by the Mars–van Krevelen mechanism is to improve the mobility of lattice oxygen to the surface and facilitate the adsorption of gaseous O_2 onto the lattice. According to the crude electron pair Lewis theory, O_V can be Lewis basic because of the electrons that are left behind at the site when the oxide ion is removed to create the vacancy.[21] This also facilitates the creation of a reactive lattice oxygen species.[43,44] Although the concentration of O_V on the surface increases with the concentration of doped Cu, the activity of oxidation catalysis seems to be dependent on the reducibility of Cu^{2+} (as shown by TPR, CV and XPS), making it an important descriptor of the activity. If the reducibility of Cu^{2+} is due to the acceptance of electrons left behind by the lattice oxygen at the O_V sites, then the basicity of O_V could be the signboard for reactivity. Thus, O_V are necessary for the reactions, but electrons available at the O_V sites (as indicated by the reducibility of Cu^{2+}) could also be necessary. In addition to this, strong Lewis acidic sites like Cu^{2+} or Cu^{+} (Fig. 6 and S7†) on the surface can chemisorb ethylene, which can be eventually oxidized to CO_2 by the reactive lattice O in a series of steps involving a carbonate intermediate. O_V are eventually annihilated by the O_2 in the feed during the process oxidizing cations.[44]

4. Conclusion

Thermal oxidation of ethylene using a Cu/TiO_2 system has been studied in detail with varying concentrations of Cu. The doping of Cu neither caused any phase separation nor affected the phase purity of TiO_2. Doping of Cu^{2+} created O_V which played an important role in the oxidation catalyst. There is a direct correlation between the concentration of doped copper and concentration of surface O_V. A strong metal–support interaction probably reduced doped Cu^{2+} to Cu^{+} at lower concentrations. As the concentration of doped Cu increased, a significant increase in the stability of Cu^{2+} was noticed. A correlation between the reducibility of Cu^{2+} and its reactivity was observed. The combination of surface cationic sites and O_V created due to the doping of Cu played a crucial role in the enhanced catalytic oxidation by Cu/TiO_2. 1% Cu/TiO_2 showed the most promising activity with the highest turnover number compared to others (0.2%, 3%, and 4% Cu/TiO_2). At 673 K, 1% Cu/TiO_2 gave a 99.5% ethylene conversion and 100% selectivity to CO_2. The reusability of 1% Cu/TiO_2 was demonstrated by a stable conversion in a stream of ethylene and air at 673 K for 24 h without any deactivation. DRIFT studies indicated that the oxidation proceeded *via* carbonate intermediates. In conclusion, Cu/TiO_2 is a promising non-noble metal oxide based catalyst for the mitigation of pollution by ethylene. Cu/TiO_2 is a promising

non-noble metal system as it is active and stable for the oxidation of ethylene.

Conflicts of interest

There are no conflicts to declare.

Acknowledgements

The author K. R. would like to thank the Ministry of Education and IIT Palakkad for an HTRA fellowship. The authors would like to thank SAIF (Sophisticated Analytical Instruments Facility) in IIT Madras for the ICP-OES analysis. The authors acknowledge the Central Instrumentation Facility (CIF) in IIT Palakkad for the chemical and material characterization. The funding of the projects 2019-017-CY-DIJ-DFRL-SP and 2020-036-CY-DIJ-SERB-SP is acknowledged. The authors thank Dr. C. P. Priyakumari (IIT Palakkad) for useful discussions.

References

1 K. B. Tran, J. J. Lang, K. Compton, R. Xu, A. R. Acheson, H. J. Henrikson, J. M. Kocarnik, L. Penberthy, A. Aali, Q. Abbas and B. Abbasi, *Lancet*, 2022, **400**, 563–591.
2 L. K. Sahu, *Curr. Sci.*, 2012, **102**, 1645–1649.
3 J. Williams and R. Koppmann, *Volatile Organic Compounds in the Atmosphere*, Blackwell Publishing Ltd, Oxford UK, 2007, vol. 1, pp. 1–32.
4 S. Sawada and T. Totsuka, *Atmos. Environ.*, 1986, **20**, 821–832.
5 A. Falls and J. Seinfeld, *Environ. Sci. Technol.*, 1978, **12**, 1398–1406.
6 W. Li, Z. Zhang, J. Wang, W. Qiao, D. Long and L. Ling, *Chem. Eng. J.*, 2016, **293**, 243–251.
7 A. Kolman, M. Chovanec and S. Osterman-Golkar, *Mutat. Res., Rev. Mutat. Res.*, 2002, **512**, 173–194.
8 H. Chen, X. Tong and Y. Li, *Appl. Catal., A*, 2009, **370**, 59–65.
9 H. G. Ahn, B. M. Choi and D. J. Lee, *J. Nanosci. Nanotechnol.*, 2006, **6**, 3599–3603.
10 D. Kumar, Y. F. Han and D. W. Goodman, *Top. Catal.*, 2007, **46**, 169–174.
11 R. J. Isaifan and E. A. Baranova, *Catal. Today*, 2015, **241**, 107–113.
12 M. Wang, L. Zhang, W. Huang, Y. Zhou, H. Zhao, J. Lv, J. Tian, X. Kan and J. Shi, *RSC Adv.*, 2017, **7**, 14809–14815.
13 E. C. Njagi, H. C. Genuino, C. K. King'ondu, S. Dharmarathna and S. L. Suib, *Appl. Catal., A*, 2012, **421**, 154–160.
14 R. Dziembaj, M. Molenda, L. Chmielarz, M. Zaitz, Z. Piwowarska and A. Rafalska-Łasocha, *Catal. Today*, 2011, **169**, 112–117.
15 M. Zhao, J. Deng, J. Liu, Y. Li, J. Liu, Z. Duan, J. Xiong, Z. Zhao, Y. Wei, W. Song and Y. Sun, *ACS Catal.*, 2019, **9**, 7548–7567.
16 H. Yang, C. Ma, Y. Li, J. Wang, X. Zhang, G. Wang, N. Qiao, Y. Sun, J. Cheng and Z. Hao, *Chem. Eng. J.*, 2018, **347**, 808–818.
17 S. Bagheri, N. Muhd Julkapli and S. Bee Abd Hamid, *Sci. World J.*, 2014, **2014**, 1–21.
18 T. Barakat, J. C. Rooke, M. Franco, R. Cousin, J. F. Lamonier, J. M. Giraudon, B. L. Su and S. Siffert, *Eur. J. Inorg. Chem.*, 2012, **2012**, 2812–2818.
19 T. Barakat, J. C. Rooke, H. L. Tidahy, M. Hosseini, J. F. Cousin, J. M. Lamonier, G. Giraudon, B. L. De Weireld and S. Su, *ChemSusChem*, 2011, **4**, 1420–1430.
20 P. Qiao, S. Xu, D. Zhang, R. Li, S. Zou, J. Liu, W. Yi, J. Li and J. Fan, *Chem. Commun.*, 2014, **50**, 11713–11716.
21 E. W. McFarland and H. Metiu, *Chem. Rev.*, 2013, **113**, 4391–4427.
22 S. Grundner, M. A. Markovits, G. Li, M. Tromp, E. A. Pidko, E. J. Hensen, A. Jentys, M. Sanchez-Sanchez and J. A. Lercher, *Nat. Commun.*, 2015, **6**, 7546.
23 J. Ren, K. H. Song, Z. Li, Q. Wang, J. Li, Y. Wang, D. Li and C. K. Kim, *Appl. Surf. Sci.*, 2018, **456**, 174–183.
24 K. Bhattacharyya, G. P. Mane, V. Rane, A. K. Tripathi and A. K. Tyagi, *J. Phys. Chem. C*, 2021, **125**, 1793–1810.
25 V. Krishnakumar, S. Boobas, J. Jayaprakash, M. Rajaboopathi, B. Han and M. Louhi-Kultanen, *J. Mater. Sci.: Mater. Electron.*, 2016, **27**, 7438–7447.
26 G. Córdoba, M. Viniegra, J. L. Fierro, J. Padilla and R. Arroyo, *J. Solid State Chem.*, 1998, **138**, 1–6.
27 M. Ikram, E. Umar, A. Raza, A. Haider, S. Naz, D. A. Ul-Hamid, J. Haider, I. Shahzadi, J. Hassan and S. Ali, *RSC Adv.*, 2020, **10**, 24215–24233.
28 S. K. S. Patel, N. S. Gajbhiye and S. K. Date, *J. Alloys Compd.*, 2011, **509**, S427–S430.
29 H. Zhu, Z. Qin, W. Shan, W. Shen and J. Wang, *J. Catal.*, 2004, **225**, 267–277.
30 S. Yuan, P. Mériaudeau and V. Perrichon, *Appl. Catal., B*, 1994, **3**, 319–333.
31 I. S. Petrik, G. V. Krylova, O. O. Kelyp, L. V. Lutsenko, N. P. Smirnova and L. P. Oleksenko, *Himia, Fizika ta Tehnologia Poverhni*, 2015, **6**, 179–189.
32 M. Liu, X. Qiu, K. Hashimoto and M. Miyauchi, *J. Mater. Chem. A*, 2014, **2**, 13571–13579.
33 J. Navas, A. Sánchez-Coronilla, T. Aguilar, N. C. Hernández, M. Desireé, J. Sánchez-Márquez, D. Zorrilla, C. Fernández-Lorenzo, R. Alcántara and J. Martín-Calleja, *Phys. Chem. Chem. Phys.*, 2014, **16**, 3835–3845.
34 B. Choudhury, M. Dey and A. Choudhury, *Int. Nano Lett.*, 2013, **3**, 1–8.
35 L. Díaz, V. D. Rodríguez, M. González-Rodríguez, E. Rodríguez-Castellón, M. Algarra, P. Núñez and E. Moretti, *Inorg. Chem. Front.*, 2021, **8**, 3491–3500.
36 Q. Ying, Y. Liu, Y. Zhang and Z. Wu, *Catal. Sci. Technol.*, 2021, **11**, 2280–2291.
37 B. T. Loveless, A. Gyanani and D. S. Muggli, *Appl. Catal., B*, 2008, **84**, 591–597.
38 A. P. Kulkarni and D. S. Muggli, *Appl. Catal., A*, 2006, **302**, 274–282.
39 L. K. Noda, R. M. de Almeida, N. S. Gonçalves, L. F. D. Probst and O. Sala, *Catal. Today*, 2003, **85**, 69–74.
40 M. R. D'Oliveira, J. Rabelo, A. G. Veiga, C. A. Chagas and M. Schmal, *Catal. Lett.*, 2020, **150**, 3036–3048.
41 H. Takano, Y. Kirihata, K. Izumiya, N. Kumagai, H. Habazaki and K. Hashimoto, *Appl. Surf. Sci.*, 2016, **388**, 653–663.

42 L. Liliana, N. Yigit, R. Rameshan, E. Kolar, D. Teschner, M. Hävecker, A. Knop-Gericke, R. Schlögl, K. Föttinger and G. Rupprechter, *ACS Catal.*, 2018, **9**, 8630–8641.
43 J. C. Mora, Y. C. M. Nederstigt, J. M. Hill and S. Ponnurangam, *J. Phys. Chem. C*, 2021, **125**, 14299–14310.
44 A. Bielański and J. Haber, *Catal. Rev.: Sci. Eng.*, 1979, **19**, 1–41.